• Basic Research •

Carnosic acid's mechanism in alleviating POAG-induced optic nerve injury *via* network pharmacology

Hao Hu, Da-Dong Jia, Li-Cheng Liang, Yi-Yao Wang, Ru-Wen Wang, Xiao-Yu Liu, Xue-Lian Guo, Liang Liang

The Second People's Hospital of China Three Gorges University, the Second People's Hospital of Yichang, Yichang 443000, Hubei Province, China

Co-first Authors: Hao Hu and Da-Dong Jia

Correspondence to: Liang Liang. The Second People's Hospital of China Three Gorges University, the Second People's Hospital of Yichang, Yichang 443000, Hubei Province, China. liangliang419519@126.com

Received: 2025-08-31 Accepted: 2025-12-01

Abstract

● **AIM:** To explore the mechanism of carnosic acid (CA) in treating primary open angle glaucoma (POAG)-induced optic nerve injury using network pharmacology and bioinformatics analyses.

● **METHODS:** CA targets were predicted using SwissTargetPrediction and TARGET PREDICTION databases, while glaucoma-related targets were identified *via* GeneCards, OMIM, DisGeNET, and CTD. Differentially expressed genes (DEGs) were identified by analyzing the Gene Expression Omnibus (GEO) dataset GSE45570, which includes optic nerve head samples from 6 POAG patients and 6 controls. Key targets were derived by intersecting DEGs with CA and glaucoma targets. The expression of the key target gene, *FABP3*, was further validated in two independent GEO datasets: GSE13534 (lamina cribrosa cells) and GSE2387 (lamina cribrosa region samples). The expression was also validated at mRNA and protein levels using quantitative real-time polymerase chain reaction (qRT-PCR) and Western blot (WB) in experimental models. Molecular docking was used to assess binding affinity, and co-immunoprecipitation (Co-IP) confirmed the interaction. Functional enrichment and immune-infiltration correlation analyses were also performed.

● **RESULTS:** A total of 306 DEGs, 84 CA targets, and 15 715 glaucoma targets were identified. FABP3 was identified as the key target, which was significantly upregulated in POAG samples in both validation datasets (GSE13534 and GSE2387) and confirmed by qRT-PCR and WB assays. Molecular docking revealed a strong binding affinity between FABP3 and CA (docking score: -9.79 kcal/mol), which was validated by Co-IP. Functional enrichment analysis showed FABP3 was associated with mitochondrial function and immune-related pathways. Correlation analysis indicated FABP3 had a significant negative correlation with activated dendritic cells (aDCs).

● **CONCLUSION:** Our study suggests that CA may treat POAG by targeting FABP3, potentially by mitigating oxidative stress and modulating immune responses. This provides a pharmacological foundation and identifies FABP3 as a potential therapeutic target for POAG treatment.

● **KEYWORDS:** primary open angle glaucoma; carnosic acid; FABP3; immune; oxidative stress

DOI:10.18240/ijo.2026.04.02

Citation: Hu H, Jia DD, Liang LC, Wang YY, Wang RW, Liu XY, Guo XL, Liang L. Carnosic acid's mechanism in alleviating POAG-induced optic nerve injury *via* network pharmacology. *Int J Ophthalmol* 2026;19(4):646-654

INTRODUCTION

Glaucoma, a leading cause of irreversible blindness worldwide, is a progressive optic neuropathy, with an estimated 111.8 million individuals projected to be affected by 2040[1-2]. Primary open angle glaucoma (POAG), the most prevalent form of glaucoma, is characterized by elevated intraocular pressure (IOP), open anterior chamber angles, and distinct morphological changes in the optic disc and retinal nerve fiber layer (RNFL)[3]. As a multifactorial genetic disorder, POAG arises from the complex interplay of multiple genes, risk factors, and endophenotypic traits[4]. Current therapeutic strategies primarily target IOP reduction; however, IOP control alone does not universally halt disease progression, as retinal ganglion cell (RGC) degeneration persists in some patients despite treatment[5-6]. As previously reported by Roberti *et al*[7], citicoline exerts a protective effect on RGCs in glaucoma patients through multiple mechanisms, including membrane stabilization, neurotransmitter modulation, anti-apoptotic effects, anti-excitotoxicity, promotion of repair, and

improvement of microcirculation. Furthermore, this drug has been shown to at least partially reverse or restore glaucomatous visual field defects. Therefore, elucidating the pathophysiology of POAG and exploring novel therapeutic interventions remain critical. Recent studies have demonstrated that inflammation[8-9] and oxidative stress[10-11] play pivotal roles in the pathogenesis of POAG, suggesting the potential therapeutic value of anti-inflammatory and antioxidant strategies in POAG management. Some natural products and their synthetic derivatives, such as ginkgo biloba extract, puerarin, and epigallocatechin gallate, have shown promising therapeutic effects in this regard[12].

Chinese herbal medicines have garnered significant attention due to their minimal adverse effects and sustained therapeutic benefits. Carnosic acid ($C_{20}H_{28}O_4$, CA), a diterpenoid compound extracted from *Labiatae* plants[13], exhibits diverse pharmacological properties, including antioxidant, anti-inflammatory, neuroprotective, and cytoprotective effects[14]. Preclinical studies have demonstrated that CA attenuates light-induced retinal oxidative stress, thereby mitigating the progression of retinitis pigmentosa and age-related macular degeneration[15]. In our previous study using a rat model of acute elevated IOP, we showed that CA treatment reduced RNFL thinning, decreased apoptotic RGCs, and increased RGC survival, suggesting its protective role against RGC apoptosis under high IOP conditions[16]. Despite these findings, the mechanisms underlying CA's therapeutic effects in POAG-associated optic nerve injury remain poorly understood.

In this study, we utilized network pharmacology to identify overlapping targets of CA and POAG, aiming to uncover potential therapeutic targets and mechanisms of CA in POAG treatment. Our findings provide a theoretical foundation for the development and clinical application of CA-based therapies for POAG-associated optic neuropathy.

MATERIALS AND METHODS

Ethical Approval All procedures received approval from the university's Experimental Animal Ethics Committee (Approval No.2025030I) and adhered to the Association for Research in Vision and Ophthalmology Statement.

Animals Forty specific pathogen-free male Sprague-Dawley mice (220-250 g) were purchased from the Laboratory Animal Center of China Three Gorges University (License No. SCXK(E)2022-0061) and housed in its barrier facility. Baseline ophthalmic examinations confirmed normal ocular findings in all mice, including red reflex, corneal clarity, anterior chamber depth, refractive state, and fundus appearance. Mice were randomly assigned to experimental or control groups. Following Jiang *et al*[6], an acute IOP model was induced in experimental mice. Under isoflurane anesthesia, anterior chamber perfusion with 0.9% sodium chloride was performed. Successful model induction was confirmed by surgical microscopy and direct ophthalmoscopy, revealing pale bulbar conjunctiva, corneal edema, retinal pallor, and interrupted retinal blood flow. Post-procedure, recovered mice were returned to the animal facility to model optic nerve damage under POAG-associated elevated IOP. At experiment completion, mice were deeply anesthetized and euthanized *via* CO_2 asphyxiation. Carcasses were disposed of by a licensed hazardous waste management company for environmentally safe treatment.

Screening of Differentially Expressed Genes in POAG The GSE45570 dataset was retrieved from the Gene Expression Omnibus (GEO) database (http://www.ncbi.nlm.nih.gov/geo/), which included optic nerve head samples from POAG patients (n=6) and age-matched control donors (n=6). DEGs between the POAG and control groups were identified using the "limma" R package (version 3.42.2) with the criteria of $|\log_2$fold change (FC)$|>0$ and P-value <0.05[17]. Additionally, volcano plots and heatmaps were generated to visualize the DEGs using the "ggVolcano" R package (version 0.02) and "ComplexHeatmap" R package (version 2.10.0), respectively[18-19].

GO Enrichment and KEGG Pathway Analysis The "clusterProfiler" R package (version 4.10.0) was utilized to perform Gene Ontology (GO) and Kyoto Encyclopedia of Genes and Genomes (KEGG) analyses on the DEGs between the POAG and control groups to elucidate their potential biological functions, with a significance threshold of $P<0.05$[20]. The enrichment results were visualized using the "ggplot2" R package.

Screening of CA Targets The chemical structure of CA was obtained from PubChem (https://pubchem.ncbi.nlm.nih.gov/) and imported into SwissTargetPrediction (http://www.swisstargetprediction.ch/; parameter: species set as "Homo sapiens") to predict potential CA targets. Additionally, CA targets were searched in TARGET PREDICTION (https://prediction.charite.de/subpages/target_prediction.php) using the keyword "carnosic acid". After merging the results, duplicates were removed, and the remaining targets were designated as CA targets for further analysis.

Screening of Glaucoma Targets Glaucoma-related targets were searched in GeneCards (https://www.genecards.org/) (parameter: category set as protein coding), Online Mendelian Inheritance in Man (OMIM; https://omim.org/), Disease Gene Network (DisGeNET; https://www.disgenet.org/; parameter: Score.gda>0), and Comparative Toxicogenomics Database (CTD; https://ctdbase.org/) using the keyword "glaucoma". After merging the results, duplicates were removed, and the remaining targets were used for subsequent analysis.

Construction of the CA-Target Network The "Venn" R package was used to perform intersection analysis and generate Venn diagrams. CA targets were intersected with glaucoma

targets to identify overlapping targets, which were then used to construct the CA-target network. The network was visualized using Cytoscape (version 3.6.1)[21]. Furthermore, overlapping targets were intersected with DEGs between the POAG and control groups to identify key targets. The expression of these key targets was validated using the GSE13534 and GSE2387 datasets from the GEO database. GSE13534 included human lamina cribrosa cells from one normal donor and one POAG donor[22], while GSE2387 comprised two optic nerve lamina cribrosa region samples from POAG patients and two from controls[23]. These datasets served as validation sets in this study.

qRT-PCR Total RNA was extracted from retinal tissue using TRIzol (Invitrogen) according to the manufacturer's instructions. cDNA was synthesized from total RNA using the QuantiTect Reverse Transcription Kit (Qiagen). Quantitative real-time polymerase chain reaction (qRT-PCR) was performed using SYBR Green Master Mix (Qiagen), with β-actin as the internal reference gene. Primer sequences were as follows: β-Actin (forward: 5'-CCATGTACGTAGCCATCC-3'; reverse: 5'-TCAGCTGTGGTGGTGAA-3') and FABP3 (forward: 5'-CGGACTTATGAGAAGGAGGC-3'; reverse: 5'-AATGTCAGAGGGGAAAACCA-3').

Western Blot Approximately 1 mL of radioimmunoprecipitation assay (RIPA) lysis buffer was added to retinal tissue and homogenized. The samples were lysed at 4°C for 30min, followed by centrifugation at 12 000 rpm for 10min. Protein concentration in the supernatant was determined using the bicinchoninic acid (BCA) protein assay kit. Approximately 20 μg of protein was mixed with 5× loading buffer, denatured in boiling water for 10min, and briefly centrifuged before loading onto a sodium dodecyl sulfate-polyacrylamide gel electrophoresis (SDS-PAGE) gel. After separation, proteins were transferred to a polyvinylidene fluoride (PVDF) membrane. To prevent nonspecific binding, the membrane was blocked with Tris-buffered saline with Tween-20 (TBST) containing blocking solution at room temperature for 1h. Primary antibodies were incubated overnight at 4°C. After incubation, the membrane was washed four times with TBST for 5min each. The membrane was then incubated with appropriate secondary antibodies at room temperature for 1h. Protein bands were visualized using an enhanced chemiluminescence (ECL) detection system.

Molecular Docking Molecular docking was performed using AutoDock to evaluate the binding affinity between key targets and CA. The crystal structure of the key target was downloaded from the PDB database (https://www.rcsb.org/; PDB ID: 1HMR). The 2D structure of CA was obtained from PubChem and converted into a 3D mol3 format file using ChemBio2D software. AutoDock (version 4.2) was used to perform molecular docking between the key target and CA, and the binding free energy was calculated. Results were visualized using PyMOL (version 2.4.1)[24].

Co-Immunoprecipitation Retinal tissue was collected and lysed in IP lysis buffer containing protease inhibitors for 40min, followed by centrifugation at 12 000 g for 10min at 4°C. The lysates were divided into Input, IgG, and FABP3 groups. Lysates were incubated with FABP3 antibody or IgG overnight at 4°C. Protein A/G magnetic beads (Beyotime) were added to the lysates and incubated at 4°C for 4h. After washing three times with IP lysis buffer, the co-precipitated proteins were analyzed by Western blot (WB).

Gene Set Enrichment Analysis Gene set enrichment analysis (GSEA) was performed to further investigate the biological functions or signaling pathways associated with key targets. Spearman correlation coefficients were calculated to assess the relationship between key targets and all genes in the GSE45570 dataset, and genes were ranked based on correlation coefficients. GSEA was conducted using the "clusterProfiler" R package (version 4.10.0; $P<0.05$), and results were visualized using "GseaVis".

Immune-infiltration Correlation Analysis Single-sample gene set enrichment analysis was performed using the "GSVA" R package (version 1.50.0) to evaluate the infiltration abundance of immune cells, immune function activity, or immune pathway activity in the POAG and control groups[25]. Additionally, Spearman correlation analysis was used to assess the relationship between immune-related gene sets and key targets ($P<0.05$).

Statistical Analysis Statistical analysis and visualization were performed using R software (University of Auckland, Auckland, New Zealand). The Wilcoxon test was used for comparisons between two groups, with a P-value <0.05 considered statistically significant.

RESULTS

Identification of Key Targets for the Treatment of POAG with CA A total of 306 DEGs were identified between the POAG and control groups, and volcano plots and heatmaps were generated to visualize these DEGs (Figure 1A-1B). To further explore the potential biological functions of the DEGs, GO and KEGG enrichment analyses were performed. GO enrichment analysis revealed that the biological processes were primarily associated with visual perception, sensory perception of light stimulus, and DNA deamination, among others (Figure 1C). Cellular component analysis indicated that the DEGs were significantly enriched in photoreceptor outer segment, non-motile cilium, and photoreceptor cell cilium (Figure 1C). For molecular function, significant enrichment was observed in terms such as deoxycytidine deaminase

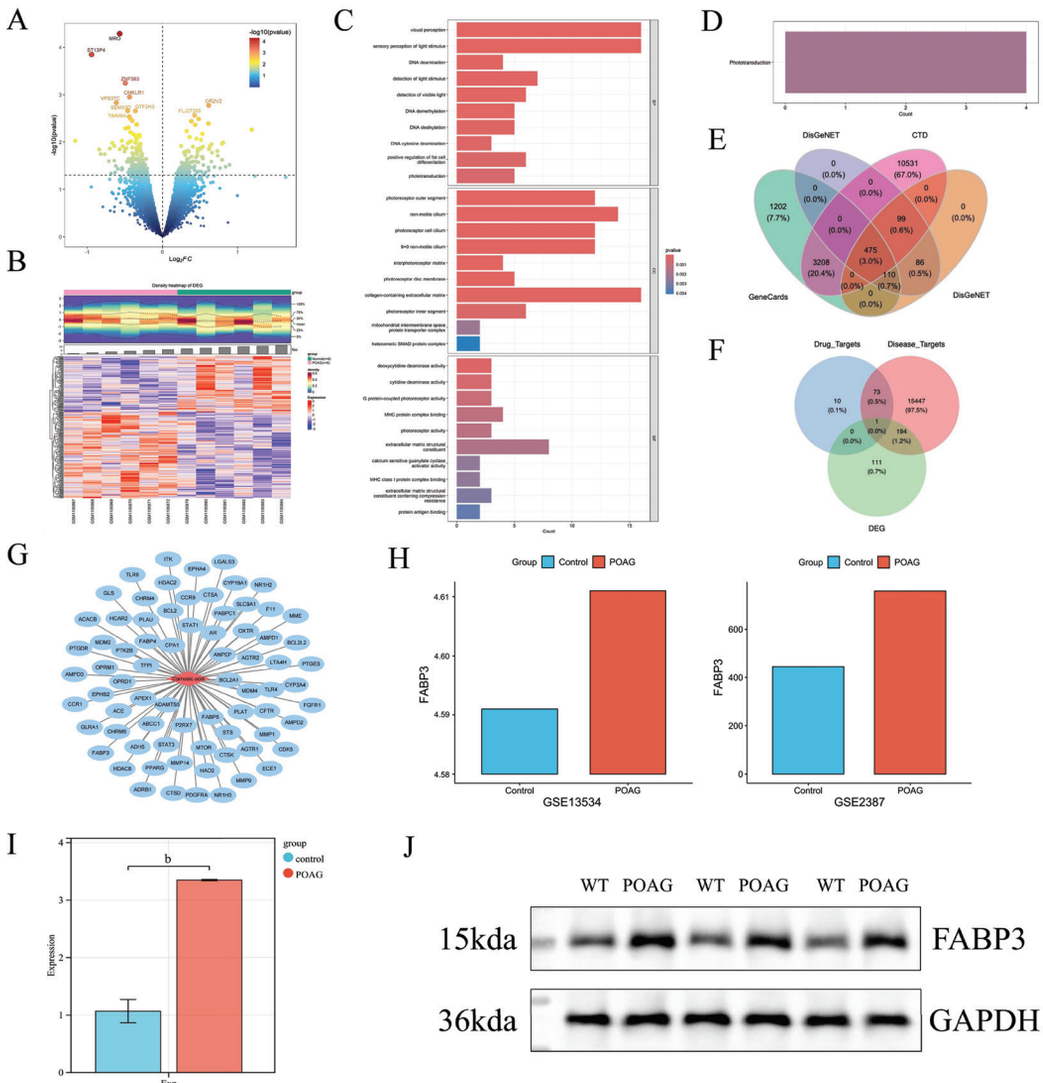

Figure 1 Identification of key targets for CA treatment for POAG A: Volcano plot of DEGs between POAG and control groups. The x-axis represents the $\log_2$FC of differential expression, and the y-axis represents the significance of the difference [$-\log_{10}$ (*P*-value)]. Each point represents a gene. Larger point size indicates a larger magnitude of differential expression (|$\log_2$FC|). Points positioned further to the right indicate genes with greater upregulation, while points further to the left indicate genes with greater downregulation. Redder color and higher position on the y-axis indicate greater statistical significance. The top 10 most significantly DEGs are labeled. B: Heatmap showing the DEGs between POAG and control groups. Each column represents a sample. The top panel shows the density distribution of relative expression levels for the DEGs. The bottom panel displays the relative expression levels of the DEGs. The left y-axis (top panel) represents relative expression level; redder color indicates a higher density of DEGs within that expression range, while bluer color indicates lower density. The left y-axis (bottom panel) lists gene names (not displayed due to large number). Hierarchical clustering based on gene expression is shown on the left. In the heatmap on the right, red blocks represent upregulated genes and blue blocks represent downregulated genes. C: Bar chart of GO enrichment analysis results. The x-axis represents the number of enriched DEGs. The y-axis lists the enriched GO terms. Terms are categorized by biological process (BP), cellular component (CC), and molecular function (MF) on the right side of the chart. Longer bars positioned further to the right indicate terms enriched with a larger number of DEGs. Redder bar color indicates greater enrichment significance. D: Bar chart of KEGG enrichment analysis results. E: Venn diagram showing the overlap of predicted targets among GeneCards, OMIM, DisGeNET, and CTD. F: Venn diagram showing the overlap of genes among DEGs, CA targets, and glaucoma targets. G: The CA-common target network. Red diamonds represent CA, blue ovals represent CA targets. Edges connecting nodes indicate potential interaction between the gene and CA. H: Box plots showing the difference in expression of FABP3 between POAG and control groups in GSE13534 and GSE2387 datasets. The y-axis represents the relative expression level of the gene. I: Bar graph of qRT-PCR assay results. The y-axis represents the relative expression level of the gene. Vertical lines above bars represent the relative SD within the group. Significance level of differences determined by *t*-test. J: Western blot bands. The first lane displays MWM. Remaining lanes show bands from samples under different conditions. Band intensity corresponds to protein expression level. $^b P<0.01$. CA: Carnosic acid; POAG: Primary open angle glaucoma; $\log_2$FC: $\log_2$fold change; DEGs: Differentially expressed genes; GO: Gene Ontology; KEGG: Kyoto Encyclopedia of Genes and Genomes; OMIM: Online Mendelian Inheritance in Man; CTD: Comparative Toxicogenomics Database; qRT-PCR: Quantitative real-time polymerase chain reaction; SD: Standard deviation; MWM: Molecular weight marker.

activity, cytidine deaminase activity, and G protein-coupled photoreceptor activity (Figure 1C). KEGG pathway analysis demonstrated that the DEGs were predominantly involved in phototransduction (Figure 1D).

Potential targets of CA were identified using SwissTargetPrediction and TARGET PREDICTION, yielding 84 potential targets after screening and deduplication. Additionally, 15 715 disease-related targets for glaucoma were obtained by integrating data from GeneCards, OMIM, DisGeNET, and CTD, followed by the removal of duplicates (Figure 1E). The intersection of CA targets and glaucoma targets revealed 74 common targets (Figure 1F). As illustrated in Figure 1G, a CA-common target network was constructed. Subsequently, one target, FABP3, was identified through the intersection of common targets and DEGs, and it was selected as a key target for CA in POAG treatment (Figure 1F). In both the GSE13534 and GSE2387 datasets, FABP3 was significantly upregulated in the POAG group (Figure 1H). Further validation by qRT-PCR (Figure 1I) and WB (Figure 1J) confirmed that FABP3 was significantly upregulated in the POAG group at both the mRNA and protein levels. These results highlight the consistent and significant role of FABP3 in POAG pathogenesis.

Prediction of CA-FABP3 Binding Capacity by Molecular Docking To assess the binding capacity between CA and FABP3, molecular docking analysis was performed. The results demonstrated that CA forms hydrogen bonds with FABP3. The docking affinity between CA and FABP3 was calculated to be -9.79 kcal/mol, indicating a strong binding affinity between FABP3 and CA (Figure 2A). Furthermore, as shown in Figure 2B, co-immunoprecipitation (Co-IP) confirmed the binding capacity between FABP3 and CA.

Enrichment Analysis for FABP3 To further investigate the potential biological functions of FABP3, GSEA was conducted. The top six enriched GO terms and KEGG pathways are presented in Figure 3A-3B. The six most significantly enriched GO terms were primarily associated with ATP synthesis coupled electron transport, mitochondrial ATP synthesis coupled electron transport, respiratory electron transport chain, antigen processing and presentation, adaptive immune response, and positive regulation of leukocyte cell-cell adhesion (Figure 3A). Enriched KEGG pathways included hematopoietic cell lineage, staphylococcus aureus infection, antigen processing and presentation, human T-cell leukemia virus 1 infection, cytokine-cytokine receptor interaction, and oxidative phosphorylation, among others (Figure 3B). In summary, these findings suggest that FABP3 is closely associated with immune regulation and mitochondrial functions.

Correlation Between Immune-Infiltration and FABP3 To further investigate the correlation between FABP3 and immune-related factors, we analyzed the associations between FABP3 and immune cells, immune functions, as well as immune pathways. The results revealed that FABP3 exhibited positive correlations with mast cells (R=0.126), regulatory T cells (Tregs; R=0.119), MHC class I (R=0.077), Th2 cells (R=0.063), and neutrophils (R=0.050; Figure 3C). Conversely, FABP3 showed negative correlations with dendritic cells (DCs; R=-0.014), activated dendritic cells (aDCs; R=-0.748), natural killer (NK) cells (R=-0.497), T cell co-inhibition (R=-0.497), Th1 cells (R=-0.441), antigen-presenting cells co-stimulation (APC; R=-0.434), C-C chemokine receptor (CCR; R=-0.420), plasmacytoid dendritic cells (pDCs; R=-0.406), cytolytic activity (R=-0.378), tumor-infiltrating lymphocytes (TIL; R=-0.357), macrophages (R=-0.322), type I IFN response (R=-0.322), inflammation-promoting factors (R=-0.301), parainflammation (R=-0.287), T cell co-stimulation (R=-0.252), immune checkpoint molecules (R=-0.245), T helper cells (R=-0.245), T follicular helper cells (Tfh; R=-0.201), Type II IFN response (R=-0.196), HLA (R=-0.175), CD8+ T cells (R=-0.147), immature dendritic cells (iDCs; R=-0.133), APC co-inhibition (R=-0.063), and B cells (R=-0.049; Figure 3C). Notably, only the correlation between FABP3 and aDCs reached statistical significance (P=0.007; Figure 3C).

DISCUSSION

In this study, the key target (FABP3) of CA for POAG treatment was identified through network pharmacology. FABPs are involved in various biological processes, including lipid metabolism, gene regulation, cell signaling, and cell proliferation and differentiation, and have been implicated in the progression of multiple neurodegenerative diseases[26-30]. For instance, arachidonic acid has been shown to promote the oligomerization of alpha-synuclein in dopaminergic neurons *via* FABP3 in Parkinson's disease pathology[31]. Additionally, FABP3 has been associated with several malignancies, such as breast cancer and gastric cancer[32-33]. Uveal melanoma, the most common primary intraocular malignancy in adults, exhibits differential expression of FABP3 between metastatic and non-metastatic cases. Knockdown of FABP3 significantly reduces the invasion and metastasis of uveal melanoma (UM) cells[34-35]. Human retinal RNA sequencing analyses have revealed that FABPs, including FABP3, FABP4, FABP5, FABP7, FABP8, and FABP12, are differentially expressed and distributed in the human retina[36-37]. However, the role of FABP3 in the pathogenesis of POAG remains unexplored.

GSEA indicated that FABP3 is associated with mitochondria-related biological processes and pathways, such as ATP synthesis coupled electron transport, mitochondrial ATP synthesis coupled electron transport, and oxidative

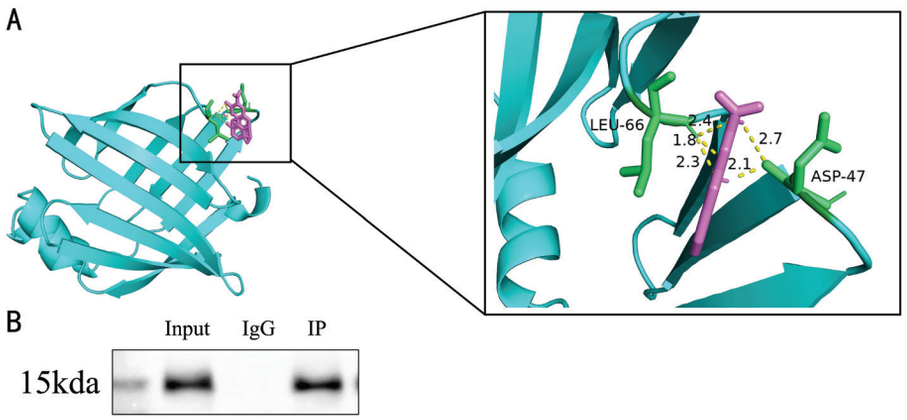

Figure 2 CA-FABP3 binding assay A: Visualization of docking between CA and FABP3 molecules (binding energy ≤-9.79 kcal/mol). Left panel: Global view of the molecular docking complex. Cyan ribbon: FABP3 protein structure (arrows indicate β-strands, helical structures indicate α-helices, lines indicate random coils). Purple sticks: Chemical structure of CA. Green sticks: Amino acid residues involved in CA binding. Right panel: Close-up view of the molecular docking interface. Yellow dashed lines indicate hydrogen bonds; numbers indicate interatomic distances in Ångstroms. B: Results of the Co-IP assay for CA and FABP3. The first lane displays the MWM. Remaining lanes show bands from samples under different conditions. CA: Carnosic acid; Co-IP: Co-immunoprecipitation; MWM: Molecular weight marker.

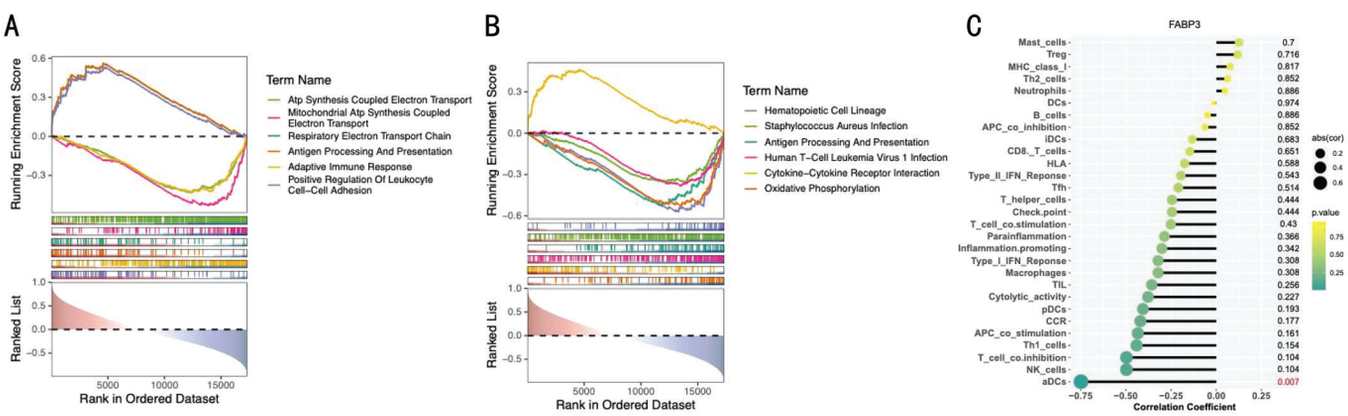

Figure 3 GSEA and correlation analysis of FABP3 A: GO enrichment analysis (GSEA); B: KEGG enrichment analysis (GSEA). For panels A and B: Top panel: GSEA enrichment plot. Y-axis: Running Enrichment Score. An enrichment curve predominantly above zero indicates a positive correlation between the gene set and FABP3 expression; a higher curve signifies stronger positive correlation. A curve predominantly below zero indicates a negative correlation; a lower curve signifies stronger negative correlation. Middle panel: Ranked list of genes for the pathway. Each vertical line represents a gene; color corresponds to the enrichment curve above and indicates membership in the gene set. Genes positioned further to the left exhibit stronger positive correlation with FABP3, while genes positioned further to the right exhibit stronger negative correlation. Bottom panel: Ranking metric plot. Y-axis: Correlation coefficient with FABP3. The curve on the left (height >0) represents genes positively correlated with FABP3; higher and redder peaks indicate stronger positive correlation. The curve on the right (height <0) represents genes negatively correlated with FABP3; lower and bluer peaks indicate stronger negative correlation. C: Lollipop chart showing the correlations between FABP3 expression and immune cell infiltration scores, immune function scores, as well as immune pathway activity scores. X-axis: Correlation coefficient (*r*) between the immune infiltration score and FABP3 expression. Y-axis: Names of immune cells, immune functions, and immune pathways. Lollipop sticks pointing left indicate a negative correlation with FABP3; sticks pointing right indicate a positive correlation. Larger circle size represents a larger absolute correlation coefficient (|*r*|). Greener color indicates a more statistically significant correlation. GO: Gene ontology; KEGG: Kyoto Encyclopedia of Genes and Genomes; GSEA: Gene set enrichment analysis.

phosphorylation. POAG is a multifactorial disease characterized primarily by the loss of optic nerve cells. RGCs, a type of central nervous system neuron, undergo degeneration in POAG, largely due to apoptosis[5]. Oxidative stress plays a significant role in the pathophysiology of RGC apoptosis by inducing mitochondrial damage[38-39]. Consequently, enhancing antioxidant defenses has shown promise in POAG treatment. For example, Inman *et al*[40] demonstrated that dietary supplementation with the natural antioxidant alpha-lipoic acid in glaucoma mice improved antioxidant gene and protein expression, protected RGCs, and enhanced axonal retrograde transport compared to controls. Coenzyme Q10, an antioxidant

cofactor for mitochondrial enzymes, regulates mitochondrial reactive oxygen species and maintains membrane integrity. In a rat model of acute retinal ischemia induced by elevated IOP, CoQ10 administration reduced glutamate excitotoxicity and RGC apoptosis[41-42]. Previous studies have shown that CA exerts neuroprotective effects by mitigating oxidative stress[43]. Specifically, CA has demonstrated cytoprotective effects against chlorpyrifos-induced inflammation, oxidative stress, and neurotoxicity in murine brain and ocular tissues, as well as in SH-SY5Y cells[44-45]. We hypothesize that the therapeutic effect of CA on POAG *via* FABP3 may be associated with alleviating oxidative stress in the optic nerve under elevated IOP.

Furthermore, FABP3 is associated with immune-related pathways, such as the nuclear factor kappa-light-chain-enhancer of activated B cells (NF-κB) signaling pathway, tumor necrosis factor (TNF) signaling pathway", and "Toll-like receptor signaling pathway". The immune system and neuroinflammation play critical roles in the development and progression of glaucomatous neurodegeneration[46]. Innate immunity is implicated in glaucoma through the activation of glial cells and oxidative stress[47]. In the aging retina, glial cells, particularly microglia, can initiate an innate immune response in response to inflammatory stimuli that oxidize proteins, lipids, and DNA[48]. While low levels of oxidative stress products are effectively cleared by microglial scavenger activity, high levels trigger microglial overactivation, leading to the excessive production of proinflammatory molecules (*e.g.*, TNFα, NF-κB, nitric oxide synthase, and cyclooxygenase-2)[49]. NF-κB, a key transcription factor in innate immunity, modulates glial cell-driven inflammatory responses, cytokine signaling, Toll-like receptor signaling, and inflammasome activation in glaucoma[50-52]. Previous studies indicate that CA activates the PI3K/AKT/NF-κB pathway, upregulating GSTP[53]. GSTP, a member of the glutathione S-transferase family, is highly expressed in glial cells of the nervous system[43]. Yu *et al*[54] demonstrated that GSTP1 polymorphisms are strongly associated with an increased risk of POAG in Caucasians. Liu *et al*[55] found reduced GSTP1 protein expression in the aqueous humor of POAG patients. We hypothesize that CA's therapeutic effect on POAG *via* FABP3 may involve immune modulation. Additionally, correlation analysis revealed a significant association between FABP3 and aDCs. DCs, as antigen-presenting cells, play a crucial role in initiating adaptive immunity[56]. However, research on adaptive immunity in glaucoma remains limited.

This study has several limitations. First, while our findings build upon our previous experimental work that showed CA's efficacy in an animal model[16], the novelty of the current research lies in its computational prediction and experimental validation of FABP3 as a direct target. However, the reliability of this prediction is inherently dependent on the quality of the public datasets used. Second, the sample size used for the experimental validation was relatively small, necessitating further analysis of additional samples to confirm the role of FABP3. Third, although we have identified and validated FABP3 as a key target, the precise downstream signaling pathways through which the CA-FABP3 interaction mitigates oxidative stress and modulates immune responses require further elucidation using more comprehensive *in vivo* and *in vitro* experiments. In conclusion, CA may target FABP3 to treat POAG by mitigating oxidative stress, as suggested by network pharmacology. This study provides a theoretical foundation for the use of CA in POAG treatment. However, additional clinical studies are needed to determine optimal dosages and validate its efficacy in real-world settings.

ACKNOWLEDGEMENTS

Foundation: Supported by the National Natural Science Foundation of China (No.81770920).

Conflicts of Interest: Hu H, None; **Jia DD,** None; **Liang LC,** None; **Wang YY,** None; **Wang RW,** None; **Liu XY,** None; **Guo XL,** None; **Liang L,** None.

REFERENCES

1 Kang JM, Tanna AP. Glaucoma. *Med Clin N Am* 2021;105(3):493-510.

2 Stein JD, Khawaja AP, Weizer JS. Glaucoma in adults—screening, diagnosis, and management: a review. *JAMA* 2021;325(2):164.

3 Park SE, Lee JS, Kim M, *et al*. What are the factors associated with the structural damage differences in open-angle glaucoma RNFL- and GCIPL-dominant progression. *J Clin Med* 2022;11(22):6728.

4 Rathi S, Danford I, Gudiseva HV, *et al*. Molecular genetics and functional analysis implicate CDKN2BAS1-CDKN2B involvement in POAG pathogenesis. *Cells* 2020;9(9):1934.

5 Kuang G, Halimitabrizi M, Edziah AA, *et al*. The potential for mitochondrial therapeutics in the treatment of primary open-angle glaucoma: a review. *Front Physiol* 2023;14:1184060.

6 Jiang RP, Lv Y, Chen BL, *et al*. Antioxidant effect of Gallic acid on retinal ganglion cells in glaucoma model. *Sci Rep* 2024;14:14907.

7 Roberti G, Tanga L, Michelessi M, *et al*. Cytidine 5'-diphosphocholine (citicoline) in glaucoma: rationale of its use, current evidence and future perspectives. *Int J Mol Sci* 2015;16(12):28401-28417.

8 Monu MN, Kumar B, Asfiya R, *et al*. Metabolomic profiling of aqueous humor from glaucoma patients identifies metabolites with anti-inflammatory and neuroprotective potential in mice. *Invest Ophthalmol Vis Sci* 2025;66(5):28.

9 Diaz-Torres S, He WX, Yu R, *et al*. Genome-wide meta-analysis identifies 22 loci for normal tension glaucoma with significant overlap with high tension glaucoma. *Nat Commun* 2024;15:9959.

10 Salvetat ML, Pellegrini F, Spadea L, *et al*. Pharmaceutical approaches to normal tension glaucoma. *Pharmaceuticals* 2023;16(8):1172.

11 Amankwa CE, Young O, DebNath B, *et al*. Modulation of

mitochondrial metabolic parameters and antioxidant enzymes in healthy and glaucomatous trabecular meshwork cells with hybrid small molecule SA-2. *Int J Mol Sci* 2023;24(14):11557.

12 Li X, Fei Z, Fei F, *et al*. Neuroprotection mediated by natural products and their chemical derivatives. *Neural Regen Res* 2020;15(11):2008.

13 Su HY, Yang F, Lu KY, *et al*. Carnosic acid ameliorates postinflammatory hyperpigmentation by inhibiting inflammatory reaction and melanin deposition. *Biomed Pharmacother* 2024;180:117522.

14 Chen XF, Wei CT, Zhao JJ, *et al*. Carnosic acid: an effective phenolic diterpenoid for prevention and management of cancers *via* targeting multiple signaling pathways. *Pharmacol Res* 2024;206:107288.

15 Bigot K, Gondouin P, Bénard R, *et al*. Transferrin non-viral gene therapy for treatment of retinal degeneration. *Pharmaceutics* 2020;12(9):836.

16 Liang L, He LY, Zhu MN, *et al*. Protective effects of carnosic acid on retinal ganglion cells in acute ocular hypertension rats. *Int Ophthalmol* 2020;40(7):1869-1878.

17 Ritchie ME, Phipson B, Wu D, *et al*. Limma powers differential expression analyses for RNA-sequencing and microarray studies. *Nucleic Acids Res* 2015;43(7):e47.

18 Mullan KA, Bramberger LM, Munday PR, *et al*. ggVolcanoR: a Shiny app for customizable visualization of differential expression datasets. *Comput Struct Biotechnol J* 2021;19:5735-5740.

19 Gu ZG, Eils R, Schlesner M. Complex heatmaps reveal patterns and correlations in multidimensional genomic data. *Bioinformatics* 2016;32(18):2847-2849.

20 Yu GC, Wang LG, Han YY, *et al*. clusterProfiler: an R package for comparing biological themes among gene clusters. *OMICS A J Integr Biol* 2012;16(5):284-287.

21 Shannon P, Markiel A, Ozier O, *et al*. Cytoscape: a software environment for integrated models of biomolecular interaction networks. *Genome Res* 2003;13(11):2498-2504.

22 Kirwan RP, Wordinger RJ, Clark AF, O'Brien CJ. Differential global and extra-cellular matrix focused gene expression patterns between normal and glaucomatous human lamina cribrosa cells. *Mol Vis* 2009;15:76-88.

23 Bhattacharya SK, Crabb JS, Bonilha VL, *et al*. Proteomics implicates peptidyl arginine deiminase 2 and optic nerve citrullination in glaucoma pathogenesis. *Invest Ophthalmol Vis Sci* 2006;47(6):2508.

24 Morris GM, Huey R, Lindstrom W, *et al*. AutoDock4 and AutoDockTools4: Automated docking with selective receptor flexibility. *J Comput Chem* 2009;30(16):2785-2791.

25 Hänzelmann S, Castelo R, Guinney J. GSVA: gene set variation analysis for microarray and RNA-Seq data. *BMC Bioinform* 2013;14(1):7.

26 Guo QY, Kawahata I, Cheng A, *et al*. Fatty acid-binding proteins 3 and 5 are involved in the initiation of mitochondrial damage in ischemic neurons. *Redox Biol* 2023;59:102547.

27 Guo QY, Kawahata I, Cheng A, *et al*. Fatty acid-binding proteins: their roles in ischemic stroke and potential as drug targets. *Int J Mol Sci* 2022;23(17):9648.

28 Ren XX, Jin CY, Li QL, *et al*. Fatty acid binding proteins-mediated mitochondrial dysfunction in the development of age-related diseases: a review. *Int J Biol Macromol* 2025;309:142913.

29 Kawahata I, Fukunaga K. Impact of fatty acid-binding proteins and dopamine receptors on α-synucleinopathy. *J Pharmacol Sci* 2022;148(2):248-254.

30 Cheng A, Jia WB, Kawahata I, *et al*. Impact of fatty acid-binding proteins in α-synuclein-induced mitochondrial injury in synucleinopathy. *Biomedicines* 2021;9(5):560.

31 Shioda N, Yabuki Y, Kobayashi Y, *et al*. FABP3 protein promotes α-synuclein oligomerization associated with 1-methyl-1, 2, 3, 6-tetrahydropiridine-induced neurotoxicity. *J Biol Chem* 2014;289(27):18957-18965.

32 Pestana RMC, Silvino JPP, Oliveira AN de, *et al*. New cardiovascular biomarkers in breast cancer patients undergoing doxorubicin-Based Chemotherapy. *Arq Bras Cardiol* 2023;120:e20230167.

33 Sierzega M, Drabik A, Sanak M, *et al*. Dissecting the importance and origin of circulating myokines in gastric cancer cachexia. *Front Endocrinol* 2024;15:1437197.

34 Ramasamy P, Murphy CC, Clynes M, *et al*. Proteomics in uveal melanoma. *Exp Eye Res* 2014;118:1-12.

35 Linge A, Kennedy S, O'Flynn D, *et al*. Differential expression of fourteen proteins between uveal melanoma from patients who subsequently developed distant metastases versus those who did not. *Invest Ophthalmol Vis Sci* 2012;53(8):4634.

36 Higashide M, Watanabe M, Sato T, *et al*. FABP5 is a possible factor for the maintenance of functions of human non-pigmented ciliary epithelium cells. *Int J Mol Sci* 2024;25(17):9285.

37 Umetsu A, Furuhashi M, Watanabe M, *et al*. Fatty acid metabolism is involved in both retinal physiology and the pathology of retinal vascular diseases. *Prostaglandins Leukot Essent Fat Acids* 2022;183:102473.

38 Jassim AH, Fan Y, Pappenhagen N, *et al*. Oxidative stress and hypoxia modify mitochondrial homeostasis during glaucoma. *Antioxid Redox Signal* 2021;35(16):1341-1357.

39 Ni YQ, Hu YY, Zhu LJ, *et al*. Lycium barbarum polysaccharide-derived nanoparticles protect visual function by inhibiting RGC ferroptosis and microglial activation in retinal ischemia–reperfusion mice. *Adv Healthc Mater* 2024;13(26):2304285.

40 Inman DM, Lambert WS, Calkins DJ, *et al*. α-lipoic acid antioxidant treatment limits glaucoma-related retinal ganglion cell death and dysfunction. *PLoS One* 2013;8(6):e65389.

41 Deppe L, Mueller-Buehl AM, Tsai T, *et al*. Protection against oxidative stress by coenzyme Q10 in a porcine retinal degeneration model. *J Pers Med* 2024;14(4):437.

42 Maiuolo J, Bulotta RM, Oppedisano F, *et al*. Potential properties of natural nutraceuticals and antioxidants in age-related eye disorders. *Life (Basel)* 2022;13:77.

43 Mirza FJ, Zahid S, Damian Holsinger RM. Neuroprotective effects of carnosic acid: insight into its mechanisms of action. *Molecules* 2023;28(5):2306.

44 AlKahtane AA, Ghanem E, Bungau SG, *et al*. Carnosic acid alleviates chlorpyrifos-induced oxidative stress and inflammation in mice cerebral and ocular tissues. *Environ Sci Pollut Res* 2020;27(11): 11663-11670.

45 de Oliveira MR, Peres A, Ferreira GC, *et al*. Carnosic acid affords mitochondrial protection in chlorpyrifos-treated sh-Sy5y cells. *Neurotox Res* 2016;30(3):367-379.

46 Giammaria S, Siesky B, Harris A, *et al*. Profiling of the peripheral blood mononuclear cells proteome by shotgun proteomics identifies alterations of immune system components, proteolytic balance, autophagy, and mitochondrial metabolism in glaucoma subjects. *ACS Omega* 2025;10(15):14866-14883.

47 Wang LX, Wei X. T cell-mediated autoimmunity in glaucoma neurodegeneration. *Front Immunol* 2021;12:803485.

48 Rao YQ, Zhou YT, Zhou WC, *et al*. mTORC1 activation in *Chx10*-specific *Tsc1* knockout mice accelerates retina aging and degeneration. *Oxid Med Cell Longev* 2021;2021:6715758.

49 Vernazza S, Tirendi S, Bassi AM, *et al*. Neuroinflammation in primary open-angle glaucoma. *J Clin Med* 2020;9(10):3172.

50 Ahmed CM, Johnson HM, Lewin AS. Corneal application of SOCS1/3 peptides for the treatment of eye diseases mediated by inflammation and oxidative stress. *Front Immunol* 2024;15: 1416181.

51 Wagner N, Reinehr S, Palmhof M, *et al*. Microglia activation in retinal ischemia triggers cytokine and toll-like receptor response. *J Mol Neurosci* 2021;71(3):527-544.

52 Harari OA, Liao JK. NF-κB and innate immunity in ischemic stroke. *Ann N Y Acad Sci* 2010;1207(1):32-40.

53 Lin CY, Chen JH, Fu RH, *et al*. Induction of pi form of glutathione *S*-transferase by carnosic acid is mediated through PI3K/Akt/NF-κB pathway and protects against neurotoxicity. *Chem Res Toxicol* 2014;27(11):1958-1966.

54 Yu YB, Weng Y, Guo J, *et al*. Association of glutathione S transferases polymorphisms with glaucoma: a meta-analysis. *PLoS One* 2013;8(1):e54037.

55 Liu AH, Wang LM, Feng Q, *et al*. Low expression of GSTP1 in the aqueous humour of patients with primary open-angle glaucoma. *J Cellular Molecular Medi* 2021;25(6):3063-3079.

56 Dai W, Zheng P, Luo DQ, *et al*. LPIN1 is a regulatory factor associated with immune response and inflammation in sepsis. *Front Immunol* 2022;13:820164.